Journal of Nuclear Materials 378 (2008) 211–219

Contents lists available at ScienceDirect

Journal of Nuclear Materials

journal homepage: www.elsevier.com/locate/jnucmat

Fracture behavior of austenitic stainless steels irradiated in PWR

K. Fukuya [a,*], H. Nishioka [a], K. Fujii [a], M. Kamaya [a], T. Miura [a], T. Torimaru [b]

[a] Institute of Nuclear Safety System Inc., 64 Sata, Mihama-cho, Mikata-gun, Fukui 919-1205, Japan
[b] Nippon Nuclear Fuel Development, 2163 Narita-cho, Oarai-machi, Ibaraki 311-1313, Japan

ARTICLE INFO

PACS:
28.41.Qb
61.80.Hg
61.80.Bg
62.20.mj
62.20.mt

ABSTRACT

Fracture behavior of cold-worked 316 stainless steels irradiated up to 73 dpa in a pressurized water reactor was investigated by impact testing at −196, 30 and 150 °C, and by conventional tensile and slow tensile testing at 30 and 320 °C. In impact tests, brittle IG mode was dominant at −196 °C at doses higher than 11 dpa accompanying significant decrease in absorbed energy. The mixed IG mode, which was characterized by isolated grain facets in ductile dimples, appeared at 30 and 150 °C whereas the fracture occurred macroscopically in a ductile manner. The sensitivity to IG or mixed IG mode was more pronounced for higher dose and lower test temperature. In uniaxial tensile tests, IG mode at a slow strain rate appeared only at 320 °C whereas mixed IG mode appeared at both 30 and 320 °C at a fast strain rate. A compilation of the results and literature data suggested that IG fracture exists in two different conditions, low-temperature high-strain-rate (LTHR) and high-temperature low-strain-rate (HTLR) conditions. These two conditions for IG fracture likely correspond to two different deformation modes, twining and channeling.

1. Introduction

It is generally recognized that austenitic stainless steels have good ductility and fracture in a ductile manner even after neutron irradiation although the uniform and total elongations are significantly reduced for higher doses. However, it is also known that neutron irradiation causes changes in fracture mode from ductile to non-ductile fracture such as intergranular (IG) fracture and channel fracture in fast breeder and fusion reactor relevant conditions [1–6]. One of such non-ductile mode is IG fracture that occurs in the creep region at temperatures higher than 0.5 Tm (Tm: melting point in K) in low-strain-rate or low stress conditions. In the IG creep fracture, wedge cracks at triple-points of grain boundaries due to grain boundary sliding or cavities on grain boundaries nucleate and grow. This type of IG fracture is known to be significantly enhanced by helium generation by nuclear transmutation reactions, as helium embrittlement. Cavities on grain boundaries are stabilized by helium and grow via stress enhanced diffusion. Another low-ductility fracture mode is transgranular channel fracture, which appears in stainless steels irradiated to doses higher than 10 dpa at temperatures higher than 370 °C and tested at temperatures lower than the creep region [5–6]. Since the channel fracture occurs only in materials containing well-developed voids, it is believed to be caused by stress concentration at voids under localized shear in dislocation channels.

Recently, non-ductile fracture modes without any environmental factor were also reported in stainless steels irradiated at ~300 °C in pressurized water reactors (PWRs) and tested at ~300 °C. Several experimental studies showed that IG fracture occurred in cold-worked 316 stainless steels (CW316 SS) and solution annealed 304 stainless steels (304 SS) irradiated to doses higher than 10 dpa in PWRs under slow tensile testing ($<10^{-7}$/s) at ~300 °C [7–11]. The IG fracture appeared from the specimen surface and the susceptibility to IG fracture increased with increasing dose and decreasing strain rate. In conventional tensile test conditions at strain rates of around 10^{-4}/s, no IG fracture was reported at ~300 °C [9,10,12] on CW316 SSs whereas the existence of cleavage-like features in the fracture surface was recently reported at room temperature at 30 and 65 dpa [10,13]. It was also reported that grain boundary facets appeared in the fracture surface after fatigue pre-cracking and fracture toughness testing at room temperature and that its fraction was higher for higher dose [13]. A study on annealed 304 stainless steels irradiated to 30 dpa revealed that the IG fracture appeared after conventional tensile tests (10^{-3}/s) at room temperature, constant load tests (700 MPa) at 340 °C, and impact tests at −196 °C and room temperature [14]. These studies suggest that austenitic stainless steels under PWR irradiation become susceptible to IG fracture in some conditions. With respect to the cause of the IG fractures, radiation-induced material changes such as hardening, grain boundary segregation, localized deformation and hydrogen were suggested as potential factors [8,9,11,13–15]. For example, stress or strain concentration at grain boundaries due to radiation-induced localized deformation, probably together

* Corresponding author. Tel.: +81 770 37 9114; fax: +81 770 37 2009.
E-mail address: fukuya@inss.co.jp (K. Fukuya).

0022-3115/$ - see front matter © 2008 Elsevier B.V. All rights reserved.
doi:10.1016/j.jnucmat.2008.06.028

with weakened grain boundary strength due to radiation-induced segregation and hydrogen, was suggested to cause the IG fracture that appears in slow tensile conditions at ~300 °C. Since the IG fracture might result in degradation of ductility and fracture toughness of materials, it is important to understand this phenomenon to evaluate the performance of PWR core components. However, knowledge on conditions such as irradiation, materials and loading, and underlying mechanisms of IG fracture is very limited.

In the present study, to get a better understanding of fracture behavior of PWR-irradiated stainless steels, mechanical tests were conducted on CW316 SSs irradiated to 2–73 dpa. Impact tests at −196, 30 and 150 °C, and conventional and slow tensile tests at 30 and 320 °C were conducted. Based on detailed fractography of the fracture surface, combined with the previous data of the same material [9,11,15–17] and literature data, conditions for non-ductile fracture and underlying mechanisms are discussed.

2. Experimental

Specimens were prepared from flux thimble tubes irradiated in a domestic 4-loop PWR (1175 GWe) for 9, 13 and 16 cycles. These tubes were made of a heat of CW316 SS. The chemical composition was Fe–0.04C–0.62Si–1.63Mn–0.022P–0.006S–12.61Ni–16.94Cr–2.22Mo in wt%. The outer and inner diameters of the tubes were 7.62 and 5.14 mm, respectively. The tubes were finally cold drawn to approximately 15% thickness reduction after solution heat treatment at 1038–1177 °C. Typical grain size was about 20–30 μm. The details of the tube material were described elsewhere [16]. In this study, experiments were conducted on specimens cut from several positions of the tubes, where the neutron doses were 2, 11, 22, 38 and 73 dpa. The irradiation temperature and dose rate were 293 °C, 6×10^{-9} dpa/s for 2 dpa, 323 °C, 2.8×10^{-8} dpa/s for 11 dpa, 323 °C, 5.4×10^{-8} dpa/s for 22 dpa, 298 °C, 7.8×10^{-8} dpa/s for 38 dpa and 305 °C, 1.5×10^{-7} dpa/s for 73 dpa. Microstructure, grain boundary segregation and hardness were already examined in the previous study [16]. The data in the previous study indicated that evolution of microstructure, segregation and hardness mainly depended on dose although both dose rate and temperature were expected to affect the evolution to some extent. Thus, data from the present five specimens basically provided dose-dependent properties.

Impact tests were carried out at liquid nitrogen temperature (−196 °C), room temperature (30 °C) and 150 °C in air. Fig. 1 shows the specimen configuration for the impact tests. A small notch of 0.2 mm in width and 2.5 mm in depth was introduced by mechanical machining. Since the impact tests were conducted using a Charpy impact test facility in a hot cell, each specimen was set into two stainless steel blocks measuring $10 \times 10 \times 25$ mm with a curved slit for fixing a specimen by screws as shown in Fig. 2. Specimens fixed to the blocks were put in liquid nitrogen (−196 °C) or in electric furnace (150 °C) for 30 min, and then impacted within several seconds on the anvil of the impact tests facility for the impact tests. The absorbed energy was determined by measuring the rising angle of the hammer after impact. Since the small curved specimens were impacted by the standard Charpy machine, the measurement error of absorbed energy was as large as ±40 J/cm^2. The fracture surface was examined by scanning electron microscopy (SEM). For some of the fractured specimens, the cross-section of the fracture surface was examined by optical microscopy to confirm the fracture mode.

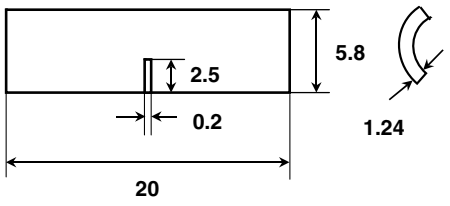

Fig. 1. Configuration of impact test specimens in mm.

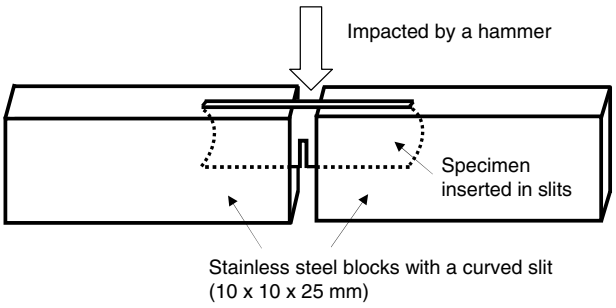

Fig. 2. Specimen setup for impact tests.

Conventional tensile tests at room temperature (30 °C) and slow tensile tests at room temperature (30 °C) and 320 °C were conducted for the 73-dpa specimen. The specimen configuration was the same as that in the previous studies [9,11]. The strain rate was set to 1.1×10^{-4}/s for conventional tensile tests and 6.7×10^{-8}/s for slow tensile tests, which were the same as in the previous studies.

3. Results

3.1. Impact tests

Fig. 3 shows examples of the typical appearance of the fracture surface. The macroscopic appearance of the fracture surface was classified into three different regions: ductile dimple region, mixed region and IG region. Fig. 4 shows a set of SEM micrographs showing the center area of the fracture surface. Fully ductile fracture occurred by shear fracture with a dimple pattern over the whole fracture surface, accompanied by macroscopic plastic deformation as shown in the top row of Fig. 3. The fracture surface was a slant fracture or combination of slant fractures, almost 45° to the tensile axis. This type of fracture appeared in the 2-dpa specimen at −196 °C, 11-dpa specimen at 30 °C, and 11- and 22-dpa specimens at 150 °C. The IG region was characterized by the existence of continuous grain facet zones. It appeared at −196 °C at doses higher than 11 dpa as shown in the bottom row of Fig. 4. The IG fracture surface was almost normal to the tensile axis. In the 11-dpa specimen tested at −196 °C, fracture initiated in ductile mode at the notch bottom and then propagated in IG mode whereas, at doses higher than 22 dpa, fracture started directly in IG mode from the notch bottom. Isolated dimples were identified on some of grain facets and became more frequent for lower dose.

The mixed region was characterized by a mixture of dimples and small isolated flat features. The flat features were 20–30 μm in size and had fine ridges that developed in one or two directions. The mixed region appeared in the center of the fracture surface and surrounded by dimple regions as shown in the middle row of Fig. 3. The area of the mixed region was larger for higher dose and lower test temperature.

To determine the nature of the flat features in the mixed region, the cross-section of the fracture surface was examined in the 73-dpa specimens after mechanical polishing and electrochemical etching in a 10% nitric acid solution to identify grain

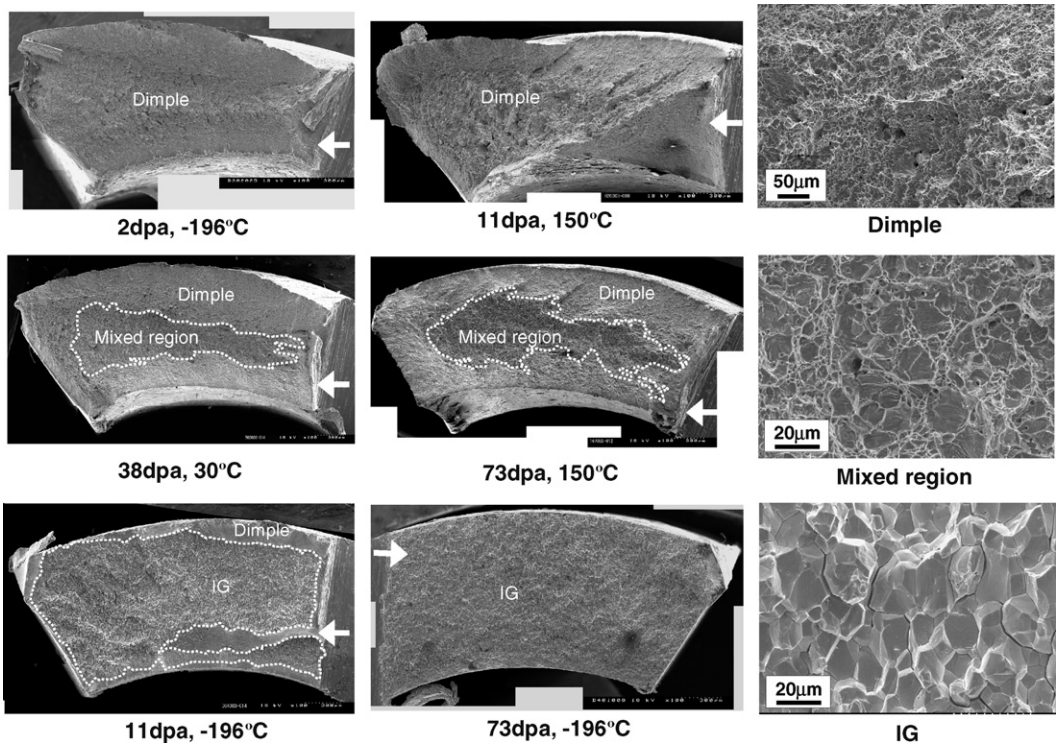

Fig. 3. Typical examples of fracture surface appearance and enlarged views of dimple, mixed region and IG after impact tests. The arrows show the notch direction.

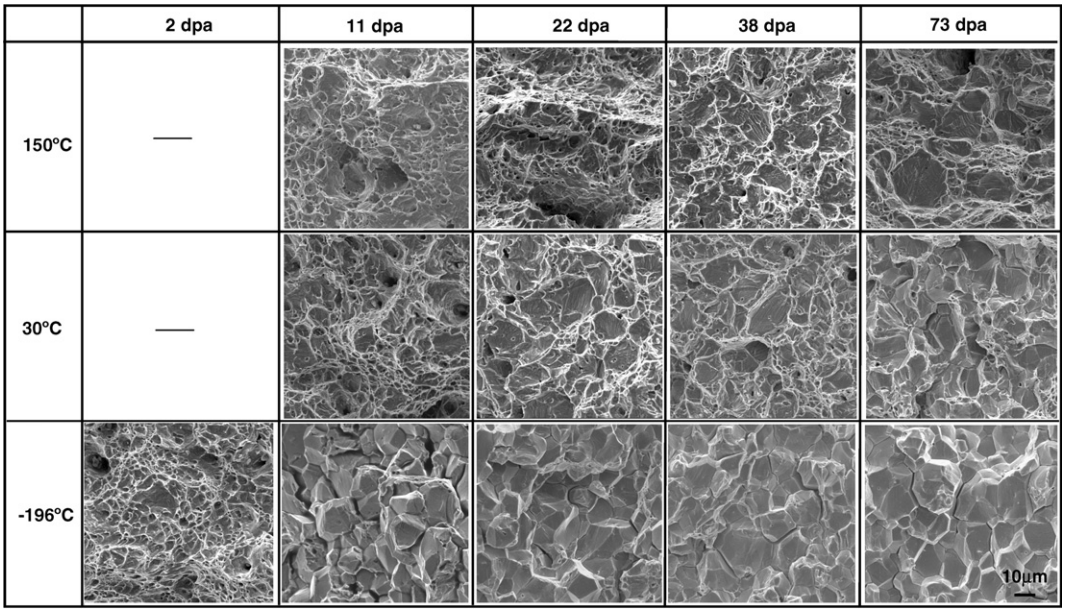

Fig. 4. Enlarged SEM micrographs showing the center of the fracture surface after impact tests.

boundaries. Fig. 5 shows optical micrographs of cross-sections together with corresponding surface appearances by SEM. The fracture surface at −196 °C showing almost full IG region was normal to the tensile axis with little reduction of the specimen thickness (Fig. 5(b)), indicating that the fracture occurred in a brittle mode. The grain facets were clearly identified as smooth straight lines in the cross-section (Fig. 5(c)). The IG region in the specimen tested at 30 °C showed cross-sections similar in appearance to that tested at −196 °C. The cross-section of the specimen tested at 150 °C showed a shear ductile fracture in general, 45° to the tensile axis, whereas the mixed region was almost normal to the tensile axis. Each flat feature in the mixed region was identified as a smooth straight line in the cross-section and was almost normal to the tensile axis. Such appearance was the same as that of grain facets observed at −196 and 30 °C. Considering this and the fact that the size of each flat feature was similar to the grain size, it is reasonable to assume that the flat feature corresponds to the grain boundary. Thus, hereafter the flat feature and mixed region are treated and described as grain facet and mixed IG region, respectively.

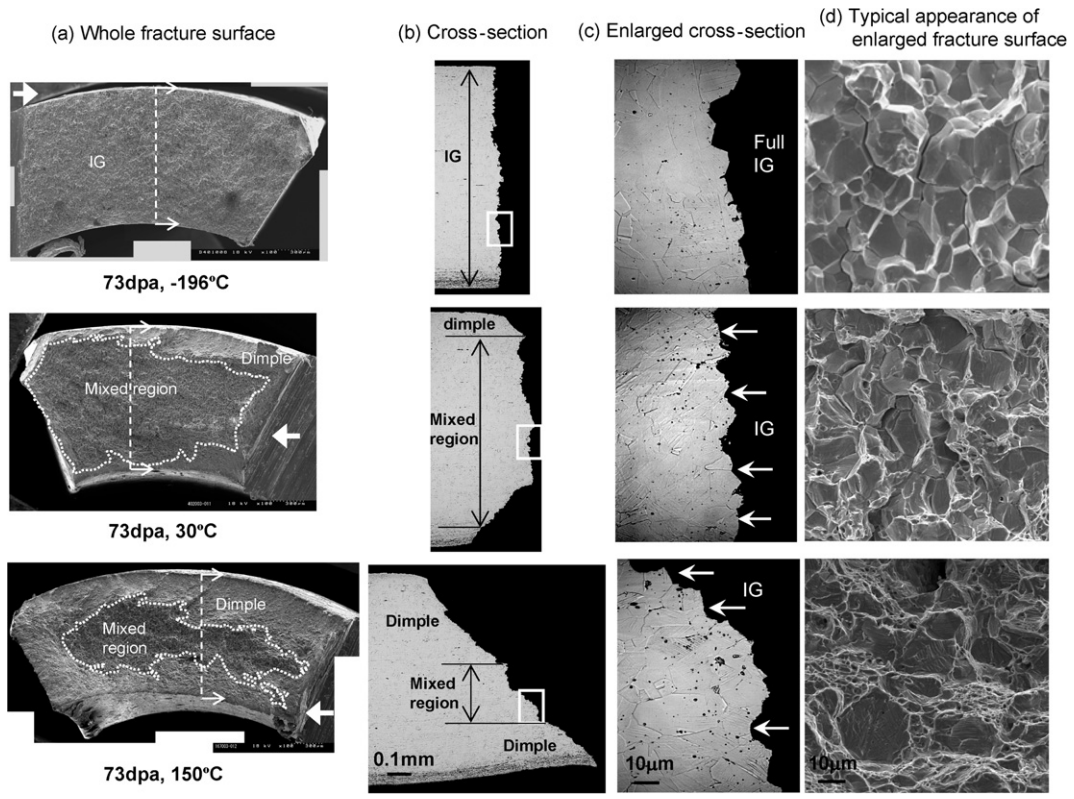

Fig. 5. Cross-sections and relevant surface appearances of fracture surfaces in the 73-dpa specimens after impact tests.

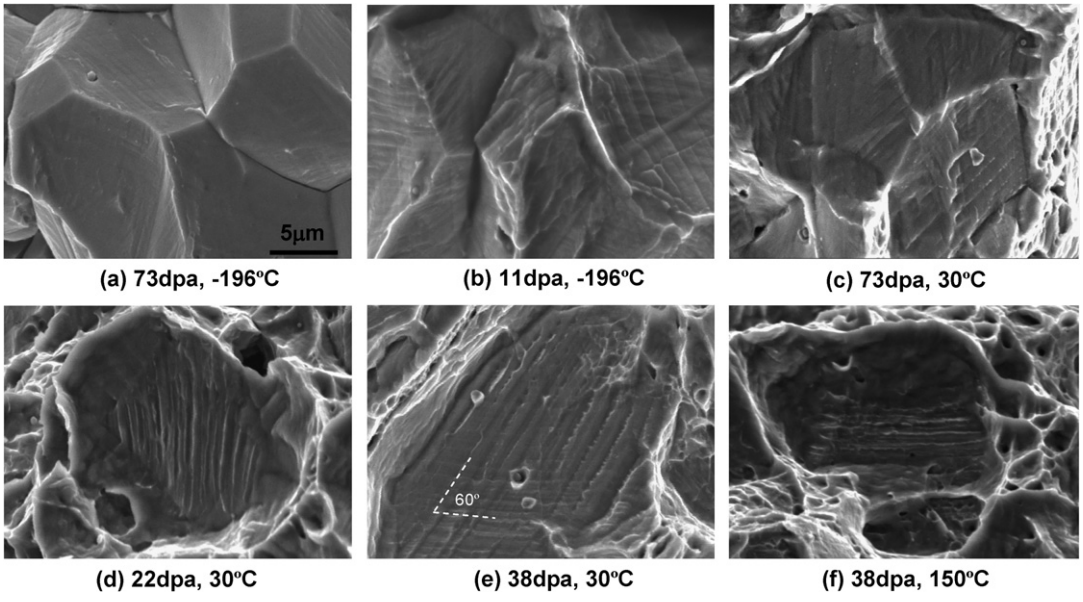

Fig. 6. Enlarged SEM micrographs showing the appearance of grain facets in the fracture surface after impact tests.

Fig. 6 shows examples of the enlarged SEM appearance of grain facets in the fracture surface. In the 73-dpa specimen, the grain facets observed after testing at −196 °C were little deformed and showed very faint traces of steps (Fig. 6(a)) whereas indication of plastic deformation and steps were clearer for lower dose (Fig. 6(b)). As seen in the bottom row of Fig. 4, isolated dimples on grain facets and opened grain boundaries became rarer for higher dose at −196 °C, indicating that plastic deformation during IG fracture reduced for higher doses. The isolated grain facets in the mixed IG region were surrounded by torn-off matrix material (Fig. 6(d)–(f)). These appearances suggest that each grain facet plays a similar role to a void in ductile dimple fracture. Hence, in the mixed IG region, cracks propagated macroscopically in a ductile manner. Each grain facet had steps or ridges in different directions to each other. The ridges in isolated grain facets showed a smooth appearance and sometimes a torn-off structure (Fig. 6(e)). The angle between two directions of steps or ridges was ~60° (Fig. 6(e)). Thus, the steps or ridges likely correspond to slips or twins on {1 1 1} planes. The

Table 1
Summary of impact test results

Dose (dpa)	Test temperature (°C)	Area fraction (%)				Absorbed energy (J/cm^2)
		Dimple	Mixed IG region	IG in mixed IG region	Net IG	
2	−196	100	0	–	0	108
11	−196	22	0	–	78	27
	30	100	0	–	0	82
	150	100	0	–	0	87
22	−196	11	0	–	89	6
	30	73	27	23	6	69
	150	100	0	–	0	75
38	−196	6	0	–	94	11
	30	73	27	33	9	70
	150	90	10	7	1	63
73	−196	1	0	–	99	6
	30	32	68	65	44	64
	150	68	32	21	7	46

spacing of steps or ridges was ~1 μm, and did not significantly differ with dose or test temperature.

Table 1 summarizes the fraction of each mode in the fracture surface and absorbed energy. In the case that the fracture surface contained the mixed IG region, the net IG fraction was determined by multiplying the fraction of mixed IG region in the whole fracture surface by the averaged area fraction of grain facets in the mixed region. The absorbed energy was determined by dividing the measured energy by the total area of fracture surface. Fig. 7 shows the dose dependence of net IG fraction and absorbed energy. The IG fraction at −196 °C was as high as 78% even at 11 dpa and became almost 100% at 73 dpa. At 30 and 150 °C, the IG fractions gradually increased with dose. The dose where the IG fracture appeared was 11 dpa at 30 °C, and 38 dpa at 150 °C. The fraction of mixed IG region, the IG fraction in the mixed region and the net IG fraction were smaller for higher test temperature at a given dose. The absorbed energy showed different trend with dose between −196 °C and, 30 and 150 °C whereas detailed comparison between 30 and 150 °C was difficult since the measurement error was large. The absorbed energy significantly decreased with increasing IG fraction at −196 °C, indicating that the IG fracture at −196 °C was actually a brittle mode. The absorbed energy at 30 and 150 °C slightly decreased with dose but was much larger than that at −196 °C. The absorbed energy in 73-dpa specimen tested at 30 °C, which showed mixed IG mode with the net IG fraction of 44%, was comparable to those of the other specimens showing mixed IG mode. This indicates that the fracture with the net IG fraction of smaller than 50% was not accompanied by notable decrease in absorbed energy in the present tests. This is likely consistent with the literature observation that the fracture toughness was not affected by the existence of a small fraction of mixed IG region [13].

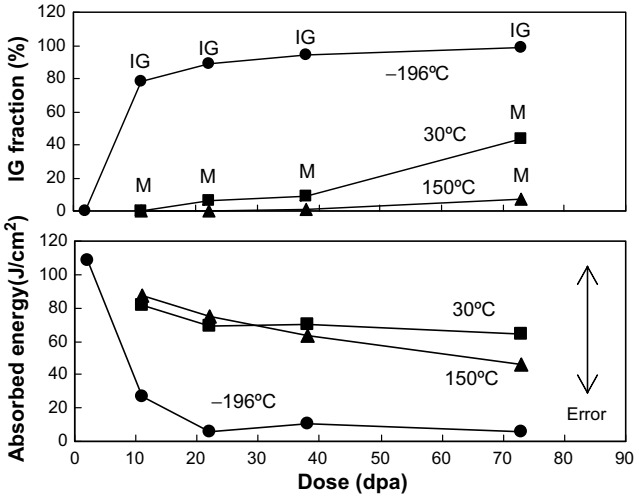

Fig. 7. Dose dependence of intergranular fraction and absorbed energy in impact tests. IG and M indicate IG mode and mixed IG mode, respectively.

3.2. Conventional tensile and slow tensile tests

Table 2 summarizes tensile test results for the 73-dpa specimens at 30 and 320 °C. Fig. 8 shows stress–elongation curves. Fig. 9 shows SEM images of the fracture surface. Since no conventional tensile test was conducted at 320 °C for the 73-dpa specimen in this study, previous data of the 53-dpa specimen and reported data at 73 dpa were used in Table 2 and Fig. 8 [9,17]. The yield strength and elongation were almost the same at 53 and 73 dpa. Fully ductile fracture was conformed at both doses. Thus, the stress–elongation curve of 73-dpa specimen is believed to be almost the same as that of 53 dpa. The uniform and total elongations in Table 2 were obtained by removing apparent elastic elongation in the stress–elongation curves. Large fluctuation of stress in the curve for the slow tensile test at 320 °C was due to fluctuations of the measurement systems.

The stress–elongation curves near the yield strength were very similar between the slow and conventional tensile tests at each temperature whereas the total elongation was slightly shorter for the slow tensile tests. Both the yield strength and elongation were larger at 30 °C than at 320 °C. A gentle decrease of the stress after general yielding at 30 °C indicated that there was no plastic instability at this temperature irrespective of strain rate, whereas plastic instability was significant at 320 °C. The fracture surface after conventional tensile tests at both 30 and 320 °C consisted of a center region containing many isolated flat features and a surrounding peripheral ductile dimple region. Although the fracture surface was generally a slant fracture, 45° to the tensile axis, the center region was almost normal to the tensile axis. The isolated flat features were 20–30 μm in size, having fine ridges that developed in one or two directions, and were surrounded by torn-off matrix material. These appearances were similar to those observed in impact tests at 30 and 150 °C. Thus, it is reasonable to assume that the flat features were grain facets and that the region was mixed IG region.

Table 2
Results of conventional and slow tensile tests

Tensile test	Dose (dpa)	Test temperature (°C)	Yield strength (MPa)	Tensile strength (MPa)	Uniform elongation (%)	Total elongation (%)	Fracture surface
Conventional	73	30	1152	1190	1.1	7.1	Mixed IG (40%)
(1.1×0^{-4}/s)	73	320	999*	1007*	0.4*	4.3*	Dimple*
	53	320	987	987	0.2	4.2	Dimple
Slow tensile	73	30	1145	1201	3.0	5.7	Mixed IG (50%)
(6.7×10^{-8}/s)	73	320	970	972	–	2.6	IG (6%)

* Data from the same tube materials tested at 3×10^{-4}/s after Takakura et al. (averaged values of two data).

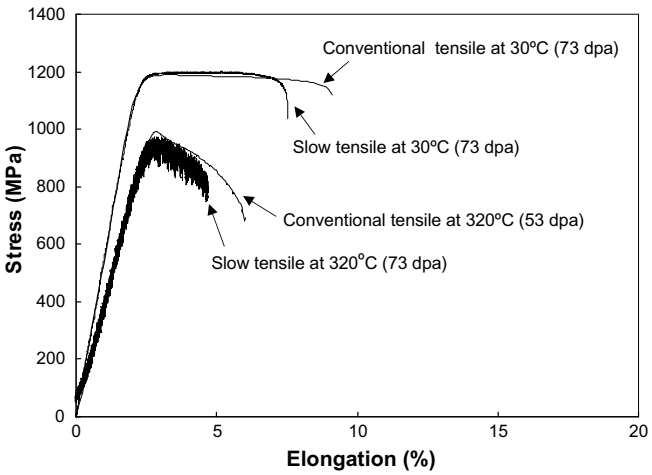

Fig. 8. Stress–elongation curves in conventional and slow tensile tests.

The fraction of mixed IG region was ~40% of the whole fracture surface at both 30 and 320 °C. Although the exact initiation position of the fracture was not clearly identified, the IG fracture likely occurred in the triaxial condition under high stress since the mixed IG region existed in the center of the cross-section of the specimen.

At 320 °C, the IG region appeared in the slow tensile tests. Although conventional tensile tests at 320 °C were not conducted in this study, the fracture mode in this condition is believed to be a full ductile mode, since no fracture mode other than ductile mode was reported for CW316 stainless steels irradiated to 30–74 dpa in conventional tensile tests at ~300 °C [9,10,13]. The IG region in the slow tensile tests at 320 °C appeared only as shallow zones along the outer and inner surfaces of the initial tube: the depth of the zones did not exceed ~100 μm. This region showed continuous IG with indication of plastic deformation such as dimples and steps on grain facets. The IG fraction was 6% at 73 dpa and did not increase with dose since the IG fraction was 3 and 4% at 35 dpa, and 3 and 13% at 53 dpa in the previous slow tensile tests at 320 °C [9].

4. Discussion

The present results confirmed that IG fracture appeared in CW316 SSs irradiated at ~300 °C in PWR under impact tests at temperatures of −196 to 150 °C, and that the susceptibility to IG fracture was higher for higher dose and lower test temperature. It was also confirmed that IG fracture appeared in conventional tensile tests only at 30 °C and slow tensile tests at both 30 and 320 °C. As mentioned in the Introduction, IG mode was recently reported in PWR-irradiated stainless steels that fractured at temperatures lower than 350 °C without any environmental factor. To understand the general characteristics of fracture behavior of stainless steels, we schematically compiled the fracture modes under various mechanical tests in air or argon environments on dose versus test temperature maps as shown in Fig. 10, based on this study and the literature [7–14]. Most of the data were for CW316 SSs, with limited data for 304 SSs. Since the experiments were conducted under various mechanical test methods, the data were divided into three sets considering strain rates: high-strain-rates in impact tests with notched specimens (typically $>10^{1}$/s), medium strain rates in conventional tensile tests (typically 10^{-5} to 10^{-2}/s) and low-strain-rates in slow tensile tests (typically $<10^{-7}$/s). Data of fracture toughness tests together with fatigue pre-cracking [13] and constant load tests [14] were additionally indicated as medium strain rate data and low-strain-rate data, respectively. The fracture mode concerning IG is plotted in three categories:

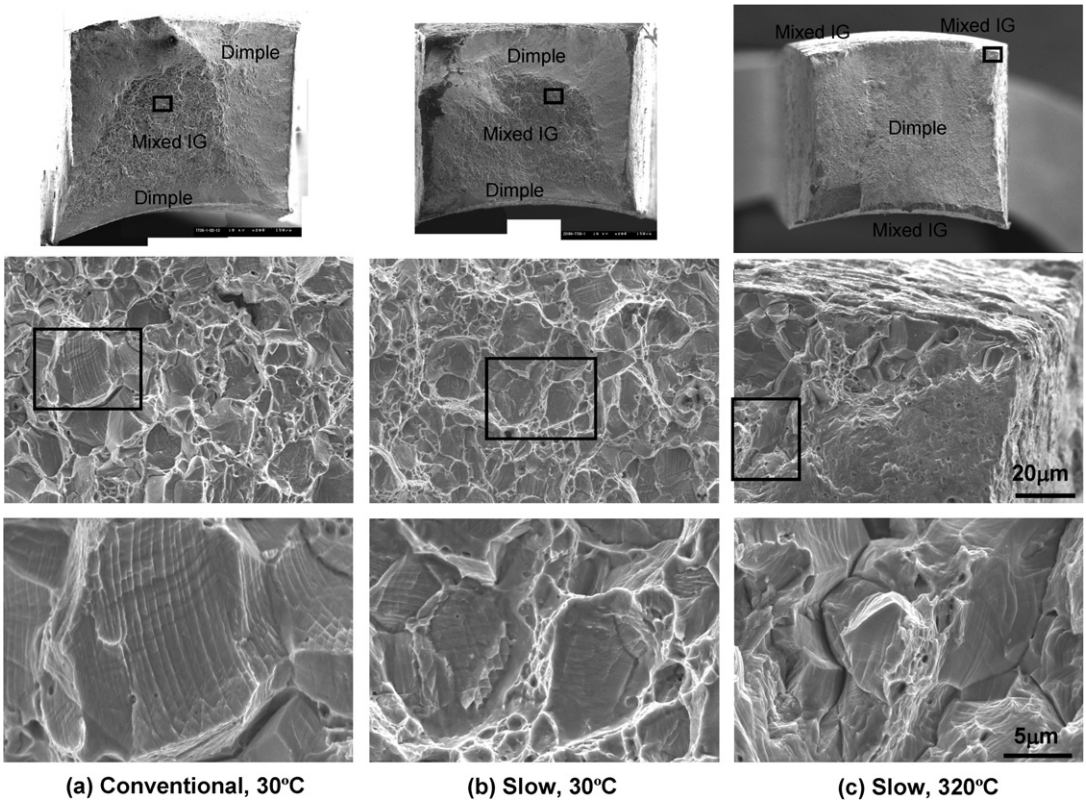

Fig. 9. Fracture surface of the 73-dpa specimens after conventional tensile tests at 30 °C and slow tensile tests at 30 and 320 °C.

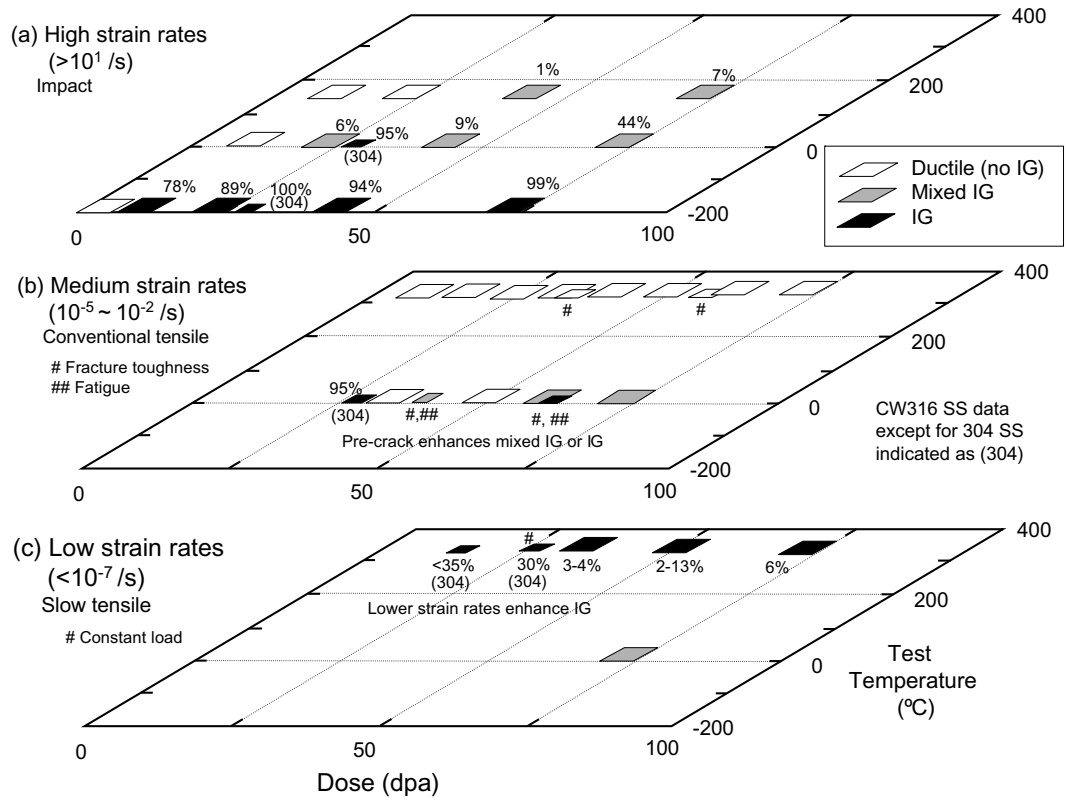

Fig. 10. Schematic plots showing fracture mode in austenitic stainless steels irradiated at ~300 °C in LWRs. The percent numbers indicate the IG fraction in the fracture surface.

ductile mode in which the fracture occurs in fully ductile mode without IG, mixed IG mode in which isolated grain facets exist in dimple regions, and IG mode in which the fracture surface contains a region of pure continuous grain facets.

In CW316 SSs, the IG mode appeared at doses as low as 11 dpa at −196 °C in high-strain-rate conditions. The IG mode and mixed IG mode appeared at higher test temperature at higher dose. In medium strain rate conditions, the IG mode never appeared at ~300 °C even at the highest dose of 73 dpa. The mixed IG mode or IG mode appeared at room temperature at higher doses. Similar IG or mixed IG mode was also observed in fatigue pre-cracking or fracture toughness tests at room temperature and observed at lower dose than in conventional tensile tests. This suggests that a higher triaxiality enhances the IG mode. In low-strain-rate conditions, the IG mode appeared at doses higher than 20 dpa at ~300 °C whereas the mixed IG mode appeared at 30 °C at 73 dpa. The data of 304 SS from a single data source [13] showed significantly higher sensitivity to IG mode than those of CW316 SSs in all conditions. This suggests that 304 SSs are more susceptible to IG mode than 316 SSs.

In the data compilation shown in Fig. 10, it is confirmed that there are two different conditions for the occurrence of IG mode in stainless steels irradiated in PWRs: low-temperature high-strain-rate (LTHR) condition and high-temperature low-strain-rate (HTLR) condition. The sensitivity to IG mode is higher for higher doses in both conditions, and becomes higher for lower temperature in LTHR conditions and for higher temperature and lower-strain-rate in HTLR conditions. The mixed IG or IG mode that appeared at 30 °C in medium and slow strain rate conditions shown in Fig. 9(a) and (b) is believed to belong to that in LTHR conditions. This is because the IG region in the 73-dpa specimen tested at 30 °C appeared in the center of the fracture surface in impact, conventional tensile and slow tensile tests, whereas the IG mode initiated from the surface in the slow tensile tests at 320 °C. The IG or mixed IG mode in LTHR conditions was enhanced by a higher triaxiality whereas the IG mode in HTLR conditions tended to occur in other conditions near the surface, probably a plane stress condition. Based on the current data shown in Fig. 10, the IG fracture in HTLR condition appeared in slow tensile tests at around 320 °C whereas the IG fracture in LTHR condition appeared at temperatures below room temperature in wide range of strain rates and also appeared at 150 °C in high dose and very high-strain-rate. There were large differences in dependence on test temperature, strain rate and stress condition as well as the range of temperature and strain rate between LTHR and HTLR conditions for the occurrence of IG fracture. This strongly suggests that the underlying mechanisms for IG fracture differ between these conditions.

The origin of the IG fracture in these two conditions is likely to be explained largely by deformation mode, based on knowledge on deformation and fracture mechanisms in irradiated stainless steels [2,13–15,18–26]. Fig. 11 shows a schematic graph showing the temperature dependence of fracture/deformation related properties and fracture mode in LTHR and HTLR conditions. The major difference in deformation is that twinning is the dominant deformation mode in LTHR conditions whereas dislocation channeling is dominant in HTLR conditions. In stainless steels highly irradiated in PWRs, stress for dislocation gliding significantly increases due to the existence of extremely dense dislocation loops and cavities. Once dislocations glide on a slip plane, moving dislocations form defect-free channels along the slip plane through interactions between dislocations and loops. Further straining causes dislocation glides that are limited to the existing channels, resulting in a decrease in stress for further dislocation gliding and then significant flow localization. Since thermal activation enhances the interaction and is more pronounced for lower strain rate at around 300 °C, channeling becomes dominant in HTLR conditions. At lower

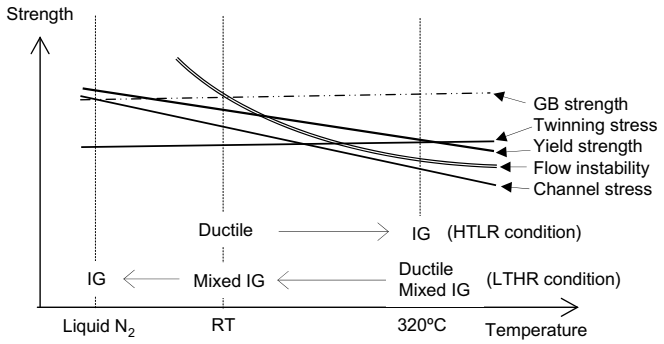

Fig. 11. Schematic graph showing temperature dependence of fracture/deformation related properties and fracture mode in highly irradiated stainless steels.

temperatures, stress for dislocation gliding becomes higher due to reduced thermal activation and exceeds the twinning stress. Since the twinning stress is lower for lower test temperature and higher strain rate, twinning is expected to become dominant in LTHR conditions. In a twinning-dominant condition, additional applied stress or strain can be accommodated by only additional twin formation and growth of existing twins. Since both the formation and growth of twins require interactions with existing dense dislocation loops, the stress for those processes remains unchanged. Thus the stress after general yielding remained unchanged and flow localization becomes insignificant, as shown in the stress–elongation curves at 30 °C in Fig. 8. Twinning is more likely in a triaxial stress condition, as observed in the previous study in which twins were dominant in the middle thickness of deformed specimens even after deformation at low-strain-rate at 320 °C whereas channeling was dominant near the surface of the same specimens [15].

The initiation of IG fracture in HTLR conditions is likely triggered by dislocation pileups in the channels. The dislocation pileup in the channels produces high stresses at grain boundaries when the channels impinge on grain boundaries. Such high stresses due to the pileups are expected to bring about grain boundary separation or microcracking as a precursor of IG fracture [15]. In the slow tensile tests at ~300 °C, IG cracks initiated from the specimen surface after general yielding and propagated deeper for lower strain rate. This is probably because slips are initiated more easily in surface grains than in inner grains. Under continuous tension to a higher strain, other fine slip systems operate, and then the crack starts to propagate in a more ductile manner leaving more indication of plastic deformation.

In LTHR conditions where twinning is dominant, grain boundary separation or microcracking initiates to relieve the stress concentration when twins impinge on the grain boundaries [27]. The process is thought to be as follows. Areas on a grain boundary between twin and grain boundary intersections first separate by high stresses and then such areas coalesce and spread on one grain facets. If such process does not occur in neighboring grains, the separated part of a grain facet is isolated and acts as a void in ductile fracture and is surrounded by torn-off matrix, as shown in Fig. 6(d)–(f). This is the case for the mixed IG mode observed in both the impact and tensile tests at temperatures higher than room temperature, where dislocation gliding also operates to some extent. If such process occurs in neighboring grains, the IG separation spreads over neighboring grains and then continuous IG fracture appears. This is the case for pure IG fracture observed in impact tests at −196 °C, where deformation mode is probably pure twinning.

Since the sensitivity to IG fracture is generated by neutron irradiation and increases with increasing dose, radiation-induced changes in materials must be the origin of the IG fracture in both LTHR and HTLR conditions. In the present CW316 SSs, details of microstructure and grain boundary microchemistry were already examined [16]. Major microstructural components in the present CW316 SSs were dense dislocation loops (10–13 nm in diameter and 1–4 × 10^{22}/m^3 in density) and helium bubble (~1 nm in diameter and ~10^{23}/m^3 in density), which saturated at doses less than 10 dpa and was stable up to 73 dpa. Both dislocation loops and bubbles uniformly distributed in grains whereas neither a denuded zone of dislocation loops nor segregation of bubbles was observed at grain boundaries. Fine γ' precipitates were also detected at doses higher than 4 dpa but were a minor component since the density was much lower than that of dislocation loops. The change in microstructure with dose coincided well with the change on hardness, which also saturated at doses of less than 10 dpa and remained unchanged up to 73 dpa. Deformation heterogeneity measured as the average spacing of coarse slips after deformation proceeded from 4 dpa to 35 dpa and saturated up to 53 dpa [15]. With respect to grain boundary segregation, enrichment of Ni and Si, and depletion of Cr and Mo rapidly increased at doses of less than 10 dpa and then proceeded very slowly up to 73 dpa. A large increase in sensitivity to IG mode from 2 dpa to 11 dpa in impact tests corresponded to a large change in microstructure, hardness and segregation up to 10 dpa. This indicates that radiation-induced material changes are essential to IG fracture, at least in LTHR conditions. However, further increase in sensitivity to IG mode at doses beyond 10 dpa seems to differ between LTHR and HTLR conditions: a very clear increase in IG fraction in LTHR conditions and no increase in HTLR conditions. In the IG mode in LTHR conditions, indication of plastic deformation became less noticeable for higher dose whereas hardness remained unchanged. Thus, one possible cause of the increase in sensitivity to IG mode is a decrease in grain boundary strength. A gentle but continuous increase in grain boundary segregation of nonmetallic elements such as P and Si with dose might cause a decrease in grain boundary strength. In the IG mode in HTLR conditions, a similar effect of grain boundary segregation is expected to operate but to a lesser extent. Hydrogen also is known to weaken grain boundary cohesion and was often supposed to play a role in IG cracking of irradiated stainless steels [8,9,28]. In the present CW316 SS, the measured amount of hydrogen was 200–500 appm at dose of 2–53 dpa [16]. However, the amount of hydrogen was not dependent on dose in the present CW316 SS, since the major source of hydrogen was considered to be corrosion related processes during irradiation in high-temperature water. Thus, hydrogen is unlikely to be responsible for the increase in sensitivity to IG fracture with dose.

Other factors to be considered are metallurgical properties which depend on material compositions. In Fig. 10, data of 304 SS showed much higher sensitivity to IG fracture than data of CW316 SSs in both LTHR and HTLR conditions. Although further experiments are needed to confirm this difference, the data suggests that the sensitivity to IG fracture is affected by material compositions. Note that there is no need to consider preexisting dislocations induced by cold work in CW316 SSs since they disappear in the early stage of irradiation [16].With respect to deformation mode, stacking fault energy (SFE) is one of the key metallurgical factors. The SFE is estimated to be 62 mJ/m^2 for the present CW316SSs and higher than the value of 20 mJ/m^2 for the 304 SS in Fig. 10, using Schramm and Reed's formulation [29]. In channeling processes dominant in HTLR conditions, a low SFE results in a larger separation between partial dislocations. Gliding dislocations in a low SFE material are difficult to cross-slip and slip in a planar manner. The slip system is, therefore, more planar in 304 SS than in 316 SS although the slip planarity is significantly high due to the existence of dense defects in highly irradiated stainless steels. Furthermore, stress induced by dislocation pileups

at channel-grain boundary intersections is expected to be larger for a low SFE material due to a larger distance between partials. Thus, it is conceptually acceptable that 304 SS with a lower SFE is more susceptible to IG fracture than CW316 SSs in HTLR conditions. In twinning processes dominant in LTHR conditions, twinning stress is proportional to SFE [24]. Thus, the twinning process operates to a higher extent in a low SFE material than in a high SFE material at a given condition. In other words, the twinning process operates at higher temperature and faster strain rate for a lower SFE material. This is consistent with the trend that 304 SS is more sensitive to IG fracture than CW316 SSs in LTHR conditions.

In LTHR conditions, especially at very low-temperature, martensite is expected to form and might make some contribution to mechanical behavior. The stability of the austenitic phase can be compared by the temperature at which 50% of the austenite is transformed to martensite during tensile tests at a true strain of 0.3 (Md_{30}). The values calculated by using Angle's formulation [30] were 256 and 300 K for the present CW316 SS and 304 SS, respectively, indicating that more martensitic phase can exist in 304 SS during deformation. Contrary to channeling, both twinning and martensite formation need nucleation and growth processes to accommodate stress in the matrix. Thus, martensite formation, if it occurs, likely plays a similar role in deformation behavior to twinning.

The present study revealed that there are two types of IG fracture mode in stainless steels irradiated in PWRs at temperatures below ~300 °C. However, experimental data are still limited for a general understanding for the conditions relevant to irradiation, material and stress/strain and underlying mechanisms of such fracture mode. Further studies are needed to clarify these points and establish a wider understanding of the fracture behavior of stainless steels including other brittle modes such as channel fracture that have been observed under higher temperature irradiation and testing conditions relevant to fast breeder and fusion applications.

5. Conclusions

Fracture behavior of cold-worked 316 stainless steels irradiated up to 73 dpa in a PWR was investigated by impact testing at −196, 30 and 150 °C, and by conventional tensile and slow tensile testing at 30 and 320 °C. In impact tests, the brittle IG mode appeared at −196 °C at doses higher than 11 dpa accompanying a significant decrease in absorbed energy. The mixed IG mode, which was characterized by isolated grain facets in ductile dimples, appeared at 30 and 150 °C whereas the fracture occurred macroscopically in a ductile manner. The sensitivity to IG or mixed IG mode was more pronounced for higher dose and lower test temperature. The IG mode appeared in slow tensile tests at 320 °C and in conventional tensile tests at 30 °C. The former initiated from the specimen surface whereas the latter appeared in the center of the fracture surface. A compilation of the results and literature data suggested that IG fracture occurs in two different conditions: low-temperature high-strain-rate (LTHR) and high-temperature low-strain-rate (HTLR) conditions. The mechanisms of IG cracking and difference in these two conditions were discussed in terms of deformation mode, and seemed to be explained to a large extent. In HTLR conditions where channeling is the dominant deformation mode, coarse channels likely cause high stresses at the intersection with grain boundaries, resulting in separation or cracks. In LTHR conditions where twinning is the dominant deformation mode, grain boundary separation or microcracking initiates to relieve the stress concentration when twins impinge on the grain boundaries. Increasing sensitivity to IG fracture with dose up to 73 dpa did not correspond to saturation of mechanical properties at ~10 dpa and gentle increase in grain boundary segregation.

References

[1] M.L. Grossbeck, J.O. Stiegler, J.J. Holme, Radiation Effects in Breeder Reactor Structural Materials, TMS-AIME, New York, 1977.
[2] M. Li, S.J. Zinkle, J. Nucl. Mater. 361 (2007) 192.
[3] G.E. Lucas, J. Nucl. Mater. 206 (1993) 287.
[4] R.L. Fish, C.W. Hunter, Irradiation Effects on the Microstructure and Properties of Metals, ASTM STP611, ASTM, 1976, p.119.
[5] M.L. Hamilton, F.-H. Huang, W.J.S. Yang, F.A. Garner, in: Thirteenth International Symposium (Part II), ASTM STP 956, ASTM, p. 245, 1987.
[6] E.E. Bloom, F.W. Wiffen, J. Nucl. Mater. 58 (1975) 171.
[7] M.P. Mannahan, R. Kohli, J. Santucci, S. Sipush, R.L. Harris, in: Trans. of Ninth International Conference on Structural Mechanics in Reactor Technology, vol. C, p. 75, 1987.
[8] T. Mastuoka, Y. Yamaguchi, T. Yonezawa, K. Nakamura, R. Fukuda, S. Shiraishi, JSME Int. J. A42 (1999) 438.
[9] K. Fukuya, M. Nakano, K. Fujii, T. Torimaru, J. Nucl. Sci. Tech. 41 (2004) 673.
[10] J. Connerman, R. Shogan, K. Fujimoto, T. Yonezawa, Y. Yamaguchi, in: Proc. of 12th Int. Conf. on Environmental Degradation of Materials in Nuclear Power Systems – Water Reactors, TMS, 2005.
[11] H. Nishioka, K. Fukuya, K. Fujii, T. Torimaru, in: Proc. of 13th International Conference on Environmental Degradation of Materials in Nuclear Power Systems, CNS, 2007.
[12] H. Arie, S. Masamori, T.R. Mager, M. Akiyama, T. Okubo, Y. Mishima, in: Proc. of ASME/JSME Nuclear Engineering Conference, vol. 2, ASME, p.101, 1993.
[13] A. Jenssen, V. Grigoriev, R. Jakobsson, P. Efsing, in: Proc. Int. Symp. on Contributions of Materials Investigation to Improve the Safety and Performance of PWRs (Fontevraud 6), French Nuclear Energy Society, p. 649, 2006.
[14] A. Toivonen, P. Aaltonen, W.Karlsen, U. Ehensten, J.-P. Massoud, J.-M. Bouesier, in: Proc. Int. Symp. on Contributions of Materials Investigation to Improve the Safety and Performance of PWRs (Fontevraud 6), French Nuclear Energy Society, 2006, p. 567.
[15] H. Nishioka, K. Fukuya, K. Fujii, Y. Kitsunai, J. Nucl. Sci. Tech. 45 (2008) 274.
[16] K. Fukuya, K. Fujii, H. Nishioka, Y. Kitsunai, J. Nucl. Sci. Tech. 43 (2006) 159.
[17] K. Takakura, K. Nakata, M. Ando, K. Fujimoto, E. Wachi, in: Proc. of 13th International Conference on Environmental Degradation of Materials in Nuclear Power Systems, CNS, 2007.
[18] K. Fukuya, M. Nakano, K. Fujii, T. Torimaru, Y. Kitsunai, J. Nucl. Sci. Tech. 41 (2004) 1218.
[19] G.S. Was, in: Proc. 11th Int. Conf. on Environmental Degradation of Materials in Nuclear Power Systems – Water Reactors, ANS, p. 965 (2003).
[20] N. Hashimoto, S.J. Zinkle, A.F. Rowcliff, et al., J. Nucl. Mater. 321 (2003) 29.
[21] S.J. Zinkle, G.E. Lucas, Fusion Materials Semi-annual Progress Reports, DOE/ER-0131/34, 2003, p. 101.
[22] X. Wu, X. Pan, J.C. Mabon, M. Li, J.F. Stubbins, J. Nucl. Mater. 356 (2006) 70.
[23] T.S. Byun, N. Hashimoto, J. Nucl. Mater. 354 (2006) 123.
[24] T.S. Byun, N. Hashimoto, K. Farrell, J. Nucl. Mater. 351 (2006) 303.
[25] J.L. Brimhall, J.I. Cole, J.S. Vetrano, S.M. Bruemmer, Mat. Res. Soc. Symp. Proc. 373 (1995) 177.
[26] E.H. Lee, T.S. Byun, J.D. Hunn, N. Hashimoto, K. Farrell, J. Nucl. Mater. 281 (2000) 65.
[27] L. Remy, Metal. Trans. 12A (1981) 387.
[28] A.J. Jacobs, in: Influence of Radiation on Material Properties, Thirteenth Int. Symp. (Part II), ASTM STP 956, ASTM, p. 239, 1987.
[29] R.E. Schramm, R.P. Reed, Metal. Trans. 6A (1975) 1345.
[30] T. Angle, J. Iron Steel Inst. 177 (1954) 165.